Permeability-porosity relationships of shallow mudstones in the Ursa Basin, northern deepwater Gulf of Mexico

Julia Schneider Reece,[1] Peter B. Flemings,[2] Brandon Dugan,[3] Hui Long,[4] and John T. Germaine[5]

Received 9 May 2012; revised 18 October 2012; accepted 22 October 2012; published 14 December 2012.

[1] In the Ursa Basin, Gulf of Mexico, in situ mudstone permeability near the seafloor declines from 1.1×10^{-16} to 5.8×10^{-19} m^2 over a depth of 578 m. We can reproduce this in situ permeability-porosity behavior through consolidation experiments in the laboratory. We use uniaxial constant-rate-of-strain consolidation experiments to measure permeability-porosity relationships and derive in situ permeabilities of 31 mudstone samples collected at Integrated Ocean Drilling Program (IODP) Sites U1324 and U1322. Although these mudstones have similar grain-size distributions, permeability at a given porosity varies significantly between the samples due to small variations in composition or fabric. We calculate an upscaled permeability relationship based on the observed permeability variation in the samples and determine a resultant large-scale permeability anisotropy of around 30. Based on this upscaled relationship and observations of in situ pressure, we calculate upward fluid flow rates of 0.5 mm/yr. We find that given the observed compressibility, permeability, and the geologic forcing at Ursa, overpressures are predicted as observed in the subsurface. The primary mechanism for overpressure generation at Ursa is sediment loading due to rapid burial. Low vertical permeabilities, accompanied by high sedimentation rates, can cause severe overpressure near the seafloor, which controls fluid flow and can reduce slope stability as observed in the Mississippi Canyon region. Such flow systems, especially at intermediate depths on passive margins, are important due to their control over macroscale behavior such as topographic gradient of continental slopes and submarine landslides, but have been largely understudied in the past.

Citation: Reece, J. S., P. B. Flemings, B. Dugan, H. Long, and J. T. Germaine (2012), Permeability-porosity relationships of shallow mudstones in the Ursa Basin, northern deepwater Gulf of Mexico, *J. Geophys. Res.*, *117*, B12102, doi:10.1029/2012JB009438.

1. Introduction

1.1. Background

[2] Permeability describes the capacity of a porous material to transmit fluid. The permeability of marine sediments can decline by 10 orders of magnitude during burial [*Neuzil*, 1994], and is controlled by grain-size distribution, grain shape, and porosity [*Carman*, 1937; *Kozeny*, 1927; *Scheidegger*, 1974; *Spinelli et al.*, 2004a]. Porosity depends on lithology and effective stress. Permeability is a driving factor in the generation of subsurface overpressure. When compressible sediments with a low permeability are rapidly loaded, pore fluids cannot drain fast enough to remain at hydrostatic pressure, consolidation of these sediments is reduced, and overpressure develops [*Gibson*, 1958]. These overpressures drive shallow fluid flow [*Dugan and Flemings*, 2000; *Dugan and Germaine*, 2008; *Flemings et al.*, 2008] including water, petroleum, and CO_2 through sediments as well as fluxes of mass, solutes, and heat between the seafloor and ocean [*Saffer and McKiernan*, 2005], may reduce slope stability [*Flemings et al.*, 2008; *Prior and Coleman*, 1982; *Stigall and Dugan*, 2010], and can result in large submarine landslides [*Dugan and Flemings*, 2002; *Prior and Suhayda*, 1979; *Sawyer et al.*, 2009]. Thus, the relationship between permeability and porosity is a key constitutive input to numerical basin models simulating fluid flow in sedimentary basins [*Bethke and Corbet*, 1988; *Dugan and Germaine*, 2008; *Hermanrud*, 1993; *Neuzil*, 1995] as well as the evolution of basin slope stability [*Dugan and Flemings*, 2002; *Stigall and Dugan*, 2010].

[1]Bureau of Economic Geology, Jackson School of Geosciences, The University of Texas at Austin, Austin, Texas, USA.
[2]Jackson School of Geosciences, The University of Texas at Austin, Austin, Texas, USA.
[3]Department of Earth Science, Rice University, Houston, Texas, USA.
[4]ExxonMobil Upstream Research Company, Houston, Texas, USA.
[5]Department of Civil and Environmental Engineering, Massachusetts Institute of Technology, Cambridge, Massachusetts, USA.

Corresponding author: J. S. Reece, Bureau of Economic Geology, Jackson School of Geosciences, The University of Texas at Austin, University Station, Box X, Austin, TX 78713, USA. (jschneider@utexas.edu)

0148-0227/12/2012JB009438

[3] The input to these forward models is usually derived from laboratory permeability measurements performed on cm-scale samples. These types of measurements are then applied in forward models that often have grid sizes that are typically much larger than cm-scale [e.g., *Bethke and Corbet*, 1988; *Stigall and Dugan*, 2010]. This requires an upscaling of permeability behavior. Among the most common techniques are the standard mathematical averaging methods: the arithmetic, geometric, and harmonic mean [*Vidstrand*, 2001]. Several other upscaling techniques that represent a wide selection of approaches have been proposed [*Neuman*, 1994; *Rubin and Gomez-Hernandez*, 1990].

[4] Many permeability measurements are performed on piston cores that are collected from within meters of the seafloor [e.g., *Fisher et al.*, 1994; *Spinelli et al.*, 2004b] and exhibit relatively high permeabilities ($>10^{-16}$ m^2). Another focus of permeability studies, especially for the last two decades, is on gas-containing shales that are deeply buried and have low permeabilities in the microDarcy (10^{-18} m^2) to nanoDarcy (10^{-21} m^2) range [e.g., *Amann-Hildenbrand et al.*, 2012; *Billiotte et al.*, 2008; *Cui et al.*, 2009; *Luffel et al.*, 1993]. However, permeability studies on sediments from the intermediate section within several hundred meters of the seafloor are less common and almost exclusively focused on subduction zone sediments such as Barbados [*Fisher and Zwart*, 1997; *Screaton et al.*, 1990; *Taylor and Leonard*, 1990; *Zwart et al.*, 1997], Costa Rica [*McKiernan and Saffer*, 2006; *Saffer and McKiernan*, 2005; *Saffer et al.*, 2000; *Screaton et al.*, 2006], Nankai [*Adatia and Maltman*, 2004; *Bourlange et al.*, 2004; *Gamage and Screaton*, 2003; *Saffer et al.*, 2011; *Skarbek and Saffer*, 2009; *Taylor and Fisher*, 1993], and Peru [*Gamage et al.*, 2005]. That detailed understanding of permeability behavior of subduction zones, and especially accretionary prisms, was driven by a recognition that there are active flow systems, where drainage and pore pressure control the macroscale behavior of the margin [e.g., *Saffer and Bekins*, 2002, 2006].

[5] Flow systems on passive margins have become an analogous focus of study, where it is increasingly understood that flow systems control macroscale behavior, for example topographic gradient of continental slopes [*Flemings et al.*, 2008] and submarine landslides [e.g., *Berndt et al.*, 2003; *Dugan and Flemings*, 2000, 2002; *Paull et al.*, 2008]. *Yang and Aplin* [1998, 2007] published permeability studies on mudstones from passive margins like the Norwegian margin, North Sea, and Caspian Sea. However, only a few Gulf of Mexico permeability studies have been published to date [*Binh et al.*, 2009; *Bryant*, 2002; *Bryant et al.*, 1975, 1986; *Dugan*, 2008; *Long et al.*, 2008; *Stump*, 1998] despite the large interest in regional petroleum resources. *Bryant et al.* [1975] and *Bryant* [2002] published permeability results on a large number of marine sediment samples with varying clay contents from all areas of the Gulf of Mexico in both shallow and deep water as well as shallow and deep subsurface. *Bryant et al.* [1986] published permeability measurements from the Mississippi Fan within 140 m below seafloor (mbsf). *Dugan* [2008] performed permeability measurements on 8 samples from Keathley Canyon from depths between 5 and 300 mbsf. Two studies analyzed whole cores from the same IODP sites in the Ursa Basin as analyzed in this study from depths down to almost 600 mbsf; *Binh et al.* [2009] measured permeability on 14 whole core samples and *Long et al.* [2008] primarily measured the compression behavior of 32 whole cores but also estimated in situ permeabilities. However, it is rare that the samples are also well characterized with respect to their composition, mineralogy, and permeability-porosity relationship, and that they are used for in situ permeability determination and upscaling purposes. *Gamage et al.* [2011] compiled permeability-porosity relationships for subduction zone sediments, however, such a detailed analysis has not been completed for passive margin sediments.

[6] Here, we present a complete data set looking at permeability of mudstones in the first 600 m below seafloor in an area where overpressure is present and the sedimentation rate is known. We use 31 uniaxial, constant-rate-of-strain consolidation experiments out of the 32 tests published by *Long et al.* [2008] to quantify the relationship between porosity and vertical permeability over a range of vertical effective stresses for sediments of varying compositions. One compression test by *Long et al.* [2008] showed wide scatter and is eliminated from our analyses here. We use the 31 individual permeability-porosity relationships to derive in situ permeabilities. Our in situ permeability estimates are updated from *Long et al.'s* [2008] published values because we use in situ porosities derived from logging-while-drilling density data under in situ pressure conditions as opposed to from the specimens themselves. We compare our permeability-porosity results with a range of other examples and explore more fully the relationship between permeability and other factors (e.g., presence of mass transport deposits or grain-size). We then develop a lower and upper bound on permeabilities based on the harmonic and arithmetic mean that describe the upscaled vertical and horizontal permeability, respectively. Given these upscaled permeability values, we explore the potential for these sediments to generate overpressure and estimate vertical flow rates in the Ursa Basin using previously directly measured pore pressures. The richness of the data set allows us to infer a comparison of laboratory-derived permeability-porosity relationships with in situ permeability-porosity trends. Our permeability results have the potential to improve the prediction of shallow and deep overpressures and flow fields, which may result in geologic hazards such as submarine slope failures.

1.2. Geologic Setting

[7] The Ursa Basin is located in the northern deepwater Gulf of Mexico, 210 km south-southeast of New Orleans, Louisiana, USA (Figure 1a). The Ursa Basin is a salt-withdrawal minibasin that is bound to the west by the Mars Ridge, a prominent north-south trending bathymetric high. Late Pleistocene shelf, shelf-margin, and turbidite deposits are sourced from the Mississippi River and termed the Eastern Depositional Complex [*Winker and Booth*, 2000]. These sediments accumulated during Marine Isotope Stages (MIS) 2–4 in response to late Wisconsinan continental glaciation [*Winker and Booth*, 2000; *Winker and Shipp*, 2002]. *Long et al.* [2011] and *Flemings et al.* [2008] performed direct pore fluid pressure measurements in the study area and found overpressures that reach 70% of the hydrostatic vertical effective stress in the first few hundred meters below seafloor, where mud volcanoes [*Ruppel et al.*, 2005] and slope failures [*Sawyer et al.*, 2007, 2009] are present.

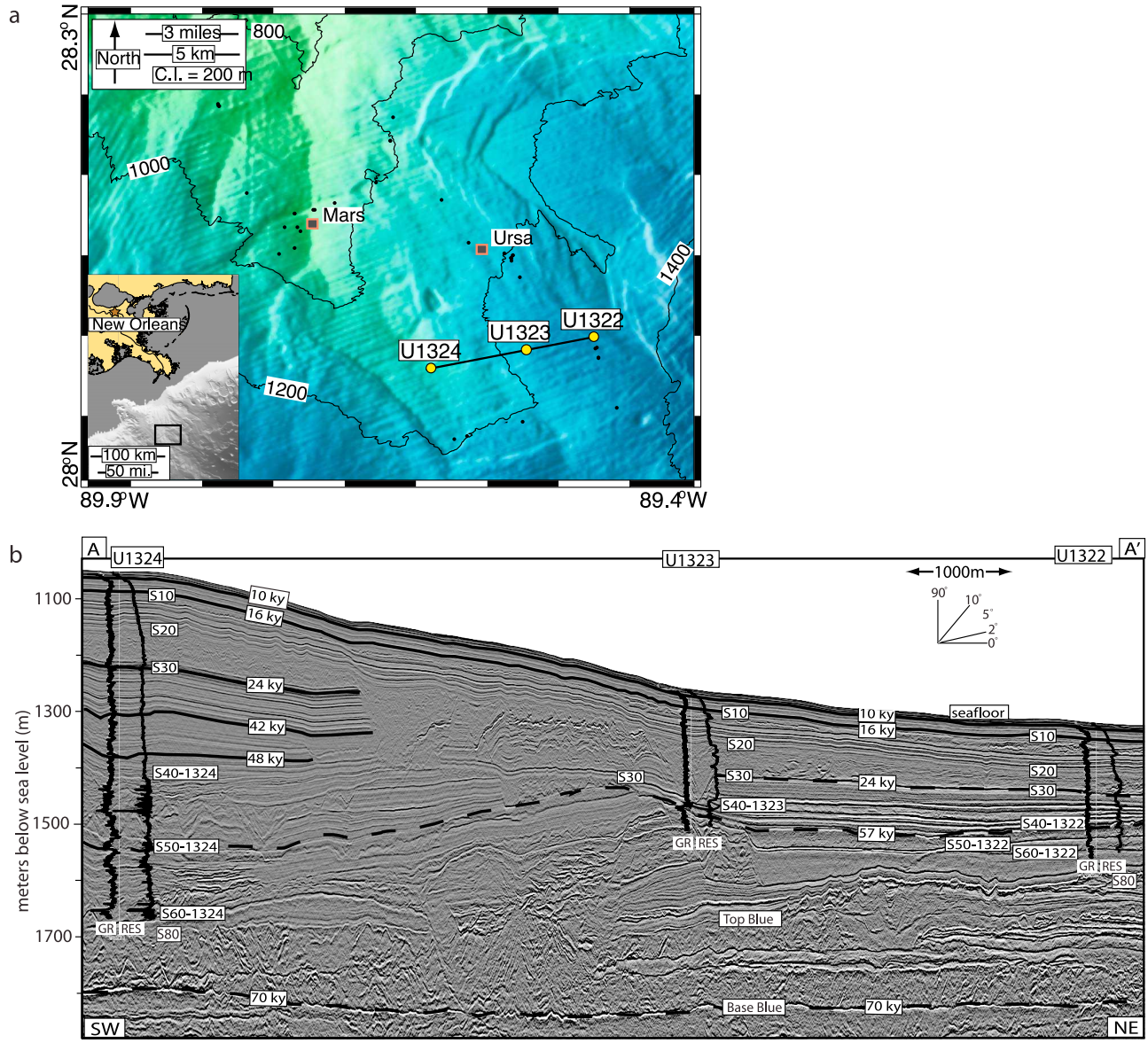

Figure 1. Study area. (a) The Ursa Region is located 210 km SE of New Orleans, Louisiana, USA (inset map). The IODP drilling transect is located in 1000–1300 m of water. IODP drill sites (yellow circles), Ursa and Mars tensionleg platforms (squares), and top-hole position industry wells (black dots) are shown (modified from *Sawyer et al.* [2009]). (b) Depth-converted seismic cross section A–A′ tied with the IODP Expedition 308 wells. Gamma ray (GR) and resistivity (RES) LWD logs are posted as well as key seismic surfaces. Solid lines represent age-equivalent horizons that have been identified at IODP sites, and dashed lines are tentative timelines (adapted from *Sawyer et al.* [2009]).

[8] Integrated Ocean Drilling Program (IODP) Expedition 308 drilled three sites in this area: U1324, U1323, and U1322 (Figure 1). Late Pleistocene deposits consist of a regional, sandstone-dominated package (the Blue Unit) overlain by channel-levee deposits and a thick package of mudstone as interpreted by *Sawyer et al.* [2007] through three-dimensional seismic data and industry well logs. These levee deposits thin to the east from ~600 m thick near Site U1324 to ~230 m thick at Site U1322 [*Flemings et al.*, 2006], and are buried by hemipelagic mudstone (Figure 1b). Multiple mass transport deposits (MTDs) are present in the channel-levee deposits. They have a high-amplitude reflection at the base, are internally seismically transparent, and are bounded by steeply dipping sidewall scarps that truncate otherwise subparallel reflectors [*Sawyer et al.*, 2007].

[9] Two characteristic lithologies are present within the mudstones above the Blue Unit: silty claystone and clayey siltstone, hereafter called Ursa Mudstone and Ursa Siltstone, respectively. The Ursa Mudstone is composed of approximately 60% (±10%) clay-size particles, 40% silt-size particles and less than 1% sand-size particles by mass determined by hydrometer analyses [*Sawyer et al.*, 2008]. The Ursa Siltstone is composed of approximately 32% clay-size particles, 67% silt-size particles, and 1% sand-size particles by

Table 1. Grain-Size Distributions by Mass[a]

CRS Number[b]	Hole-Core-Section	Depth[c] (mbsf)	% Sand[d]	% Silt[d]	% Clay[d]
CRS 21	U1322D-3H-3WR	103.44	0.07	48.21	51.72
CRS 796	U1322D-2H-2WR	72.00	0.00	41.00	59.00
CRS 798	U1322D-2H-2WR	72.00	0.40	41.40	58.20
CRS 808	U1322B-15H-1WR	125.80	0.00	29.60	70.40
CRS 810	U1322B-18H-6WR	158.01	0.70	33.70	65.60
CRS 815	U1322B-4H-3WR	27.17	0.40	34.10	65.50
CRS 824	U1322B-25H-6WR	209.13	0.03	38.88	61.09
CRS 825	U1322B-21H-3WR	-	-	-	-
CRS 826	U1322D-1H-2WR	-	-	-	-
CRS 01	U1324C-6H-3WR	304.02	0.11	37.09	62.80
CRS 02	U1324C-6H-3WR	303.94	0.03	36.37	63.60
CRS 03	U1324C-1H-2WR	51.21	0.01	44.10	55.89
CRS 04	U1324C-1H-1WR	51.14	0.04	42.59	57.37
CRS 05	U1324B-13H-7WR	117.40	0.03	40.07	59.90
CRS 06	U1324B-70X-6WR	578.13	0.03	38.17	61.80
CRS 07	U1324B-60X-2WR	476.86	0.02	41.18	58.80
CRS 08	U1324C-7H-1WR	405.81	1.54	66.73	31.73
CRS 13	U1324B-4H-7WR	32.14	0.70	34.20	65.10
CRS 14	U1324B-4H-7WR	32.10	0.00	44.70	55.30
CRS 15	U1324B-7H-7WR	60.62	0.00	50.40	49.60
CRS 18	U1324B-26H-3WR	220.34	0.00	34.00	66.00
CRS 19	U1324B-31H-3WR	261.02	0.03	41.26	58.71
CRS 20	U1324B-21H-3WR	183.14	0.31	55.04	44.65
CRS 797	U1324C-1H-1WR	51.10	0.00	34.60	65.40
CRS 799	U1324C-1H-1WR	51.10	0.00	31.90	68.10
CRS 800	U1324B-4H-7WR	31.86	0.00	44.50	55.50
CRS 801	U1324B-16H-5WR	142.10	0.00	42.00	58.00
CRS 802	U1324B-7H-7WR	60.31	0.00	39.00	61.00
CRS 803	U1324B-15H-5WR	134.20	0.30	37.70	62.00
CRS 807	U1324C-2H-4WR	104.50	0.00	49.20	50.80
CRS 812	U1324B-23H-5WR	199.80	0.50	37.30	62.20
CRS 813	U1324B-10H-7WR	88.80	0.00	39.70	60.30

[a]Notes: CRS 08 sample = Ursa Siltstone, remaining samples = Ursa Mudstone.
[b]CRS Number: constant-rate-of-strain (CRS) consolidation test performed on either the sample as used for grain-size analysis or nearby.
[c]Depth: depth of grain-size sample in meters below seafloor (mbsf) by *Sawyer et al.* [2008].
[d]% Sand, % Silt, % Clay: grain-size distributions measured by *Sawyer et al.* [2008].

mass determined by hydrometer analyses [*Sawyer et al.*, 2008].

2. Materials and Methods

2.1. Sample Descriptions

[10] Permeability was measured on nine whole cores from Site U1322 between 27 and 210 mbsf and on 22 whole cores from Site U1324 between 32 and 578 mbsf. The cores were recovered by advanced piston coring (APC) and extended core barrel (XCB) coring. Cores reserved for experiments were sealed in core liners with end caps and electrical tape and immediately refrigerated until use to keep the original water content. One sample out of the 31 whole cores is an Ursa Siltstone, the remaining 30 samples are Ursa Mudstones. The grain-size distributions are found in Table 1. Based on quantitative X-ray mineralogy, illite and smectite are the dominant minerals in the Ursa Mudstone samples and together comprise 37–60% of the bulk rock [*Long et al.*, 2008]. Analysis of the clay-size fraction (<2 μm) shows that 80–90% of the mixed-layer interlayers are composed of smectite [*Long et al.*, 2008].

2.2. Uniaxial Consolidation Experiments

[11] Uniaxial, constant-rate-of-strain (CRS) consolidation experiments are commonly used to derive compression and permeability behavior as well as preconsolidation stress [*Sheahan and Watters*, 1997]. Here, we use CRS tests to determine the change in permeability with porosity over large effective stress ranges. The CRS tests on our 31 Ursa samples were run in three different laboratories (The Pennsylvania State University, Rice University, and Massachusetts Institute of Technology) and the results were published by *Long et al.* [2008]. In these CRS tests, the samples were compressed perpendicular to bedding, thus, only vertical permeability is analyzed here. Fixed-diameter rings were used in the test setup to maintain uniaxial strain. Axial load, specimen height, and pore fluid pressure at the top and base of the specimen were monitored throughout the test. By using linear CRS theory [*Smith and Wahls*, 1969], which assumes a constant coefficient of volume change over small strains, the hydraulic conductivity, and thus, permeability is directly calculated [*ASTM International*, 2006; *Long et al.*, 2008; *Tan et al.*, 2006].

3. Results

[12] As observed in previous studies [e.g., *Gamage et al.*, 2011; *Neuzil*, 1994], the log of permeability is proportional to porosity for each of the CRS experiments (Figure 2). Vertical permeabilities of the Ursa Mudstones range over an order of magnitude at a given porosity (Figure 2). The single Ursa Siltstone sample has a permeability that is about one order of magnitude larger than the highest vertical permeability estimated in the Ursa Mudstone at a given porosity.

[13] We quantify the permeability-porosity relationships of all 31 samples by assuming a log linear behavior as often observed in porous materials [e.g., *Bryant et al.*, 1975; *Neuzil*, 1994]:

$$\log(k) = \gamma n + \log(k_0), \tag{1}$$

where γ is the permeability index and $\log(k_0)$ the y-intercept at zero porosity. For each experiment we use a least squares regression of our experimental data, over the portion of the test that corresponds to the virgin consolidation line, to estimate γ and $\log(k_0)$. Table 2 lists permeability properties for all 31 Ursa samples. We find that the slopes (γ) and the y-intercepts [$\log(k_0)$] of all permeability-porosity relationships vary with standard deviations of 1.4 and 0.9, respectively (Figure 2 and Table 2). The coefficients of the single Ursa Siltstone permeability-porosity relationship are γ = 8.60 and $\log(k_0) = -19.63$.

[14] In a CRS test, permeability can only be measured in steady state conditions, which are often reached after the sample has consolidated to its maximum past vertical effective stress. At the start of CRS loading, a time dependent variation in strain distribution within the specimen causes a transient effect [*ASTM International*, 2006]. Therefore, we obtain in situ permeabilities by extrapolating the permeability-porosity relationships observed during the CRS experiments [γ and $\log(k_0)$] back to the in situ porosities (n_i) (Table 2). We determine in situ porosity (n_i) from the logging-while-drilling (LWD) bulk density log, assuming a grain density of 2740 kg/m^3 [*Long et al.*, 2008] and

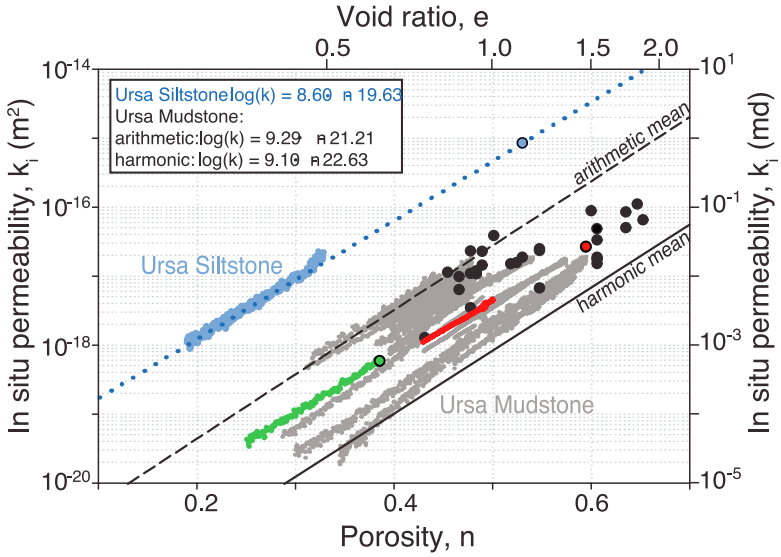

Figure 2. Log linear permeability-porosity relationships of Ursa Siltstone (light blue) and Ursa Mudstone (gray) measured in uniaxial constant-rate-of-strain (CRS) consolidation tests. Red data set is from shallow Ursa Mudstone sample (CRS 802, 60.31 mbsf) and green data set is from deepest Ursa Mudstone sample (CRS 06, 578.13 mbsf). In situ permeabilities (colored circles) are predicted by extrapolating permeability-porosity relationships to in situ porosities derived from logging-while-drilling (LWD) bulk density log. Dotted line- single Ursa Siltstone data set regression; dashed line- arithmetic mean of 30 Ursa Mudstone samples; solid line- harmonic mean of 30 Ursa Mudstone samples.

fluid density of 1024 kg/m^3 [*Long et al.*, 2008]. This contrasts the approach used by *Long et al.* [2008], where porosity was determined by using wet and oven-dried masses of the specimen itself (often termed the Moisture and Density (MAD) measurement after *Blum* [1997]). The porosity estimated from the density log is consistently 2 to 5 porosity units less than that measured either by shipboard MAD techniques or measured with the MAD technique on the CRS specimens or trimmings in the laboratory. This is commonly observed and the primary reason for this difference is that when the cores are removed from in situ conditions they are unloaded and as a result they expand. In fact, the CRS unloading curve, which describes the elastic rebound, of the sample with the highest past vertical effective stress suggests a rebound in porosity from in situ conditions to atmospheric conditions of 5%. We interpret that the porosity interpreted from the LWD log is the more accurate measure of the in situ porosity even though we are forced to estimate the grain density. The difference in porosity estimated by the two approaches is significant: our in situ permeabilities are up to 4× lower than those interpreted by *Long et al.* [2008].

[15] At Site U1324, Ursa Mudstone in situ permeabilities vary from 1.1×10^{-16} to 5.8×10^{-19} m^2 (Figures 2, 3, and 4 and Table 2). Ursa Siltstone in situ permeability is 8.5×10^{-16} m^2, more than one order of magnitude higher than Ursa Mudstone in situ permeabilities at similar porosity (Figures 2, 3, and 4). The log-derived porosity at Site U1324 decreases from 0.8 to 0.45 within the first 150 mbsf, which correlates to a reduction in in situ permeability from about 10^{-16} to about 10^{-17} m^2 (Figure 4). From 150 to 578 mbsf, porosity only decreases from 0.45 to 0.4. However, in situ permeability continues to decrease by approximately 1.5 orders of magnitude to 5.8×10^{-19} m^2 (Figure 4).

[16] At Site U1322, Ursa Mudstone in situ permeabilities vary from 6.5×10^{-17} to 3.5×10^{-18} m^2 (Figures 2, 3, and 5 and Table 2). The log-derived porosity at Site U1322 decreases from 0.9 to 0.45 within the first 120 mbsf, which correlates to a reduction in in situ permeability of half an order of magnitude from 6.5×10^{-17} to 1.5×10^{-17} m^2 (Figure 5). At 120 mbsf, which coincides with the bottom of a pronounced mass transport deposit (MTD), porosity sharply increases from 0.45 in the MTD to about 0.52 just below the MTD (Figure 5) due to the sediment densification at the bottom of the MTD [*Dugan*, 2012; *Sawyer et al.*, 2009]. From 120 to 216 mbsf, porosity decreases back to 0.45 and stays constant, which correlates to a further reduction in in situ permeability from 1.5×10^{-17} to 3.5×10^{-18} m^2 (Figure 5). Fifteen out of the 31 cores used in this study are from MTDs. There is no significant difference in in situ permeability-porosity trends between samples from MTDs and non-MTDs [*Schneider*, 2011] (Figure 6).

4. Discussion

[17] Ursa Mudstone in situ permeabilities fall within the range of permeability versus porosity measurements compiled by *Neuzil* [1994] (Figure 3, shaded region) and are in good agreement with in situ permeabilities of other samples from the Gulf of Mexico such as from Keathley Canyon [*Dugan*, 2008] and Eugene Island [*Stump*, 1998] (Figure 3, stars and hexagon, respectively). *Binh et al.* [2009] did not determine in situ permeabilities but published permeability and porosity measurements from the same Ursa Basin sites, determined by CRS tests and incremental loading tests, that range from 10^{-19} to 10^{-16} m^2 for porosities of 0.3 to 0.7, respectively (Figure 3, downward pointing triangles). Our Ursa Mudstone in situ permeabilities fall within this data

Table 2. Permeability Properties[a]

CRS Number[b]	MTD[c]	Hole-Core-Section	Depth[d] (mbsf)	ρ_b[e] (kg/m^3)	n_i[f]	γ[g]	log (k_0)[h] (m^2)	k_i[i] (m^2)
CRS 21	X	U1322D-3H-3WR	103.44	1880	0.50	10.95	−21.90	3.87E-17
CRS 796		U1322D-2H-2WR	72.78	1800	0.55	8.34	−21.74	6.74E-18
CRS 798		U1322D-2H-2WR	72.83	1800	0.55	9.78	−21.99	2.33E-17
CRS 808		U1322B-15H-1WR	126.28	1850	0.52	7.67	−20.80	1.51E-17
CRS 810	X	U1322B-18H-6WR	157.42	1910	0.48	11.05	−22.27	1.19E-17
CRS 815		U1322B-4H-3WR	27.21	1620	0.65	10.04	−22.74	6.50E-17
CRS 824	X	U1322B-25H-6WR	209.81	1920	0.48	10.07	−22.27	3.48E-18
CRS 825	X	U1322B-21H-3WR	178.70	1920	0.48	10.74	−21.77	2.30E-17
CRS 826	X	U1322D-1H-2WR	42.87	1700	0.61	9.20	−22.05	3.36E-17
CRS 01		U1324C-6H-3WR	304.02	1900	0.49	9.00	−21.05	2.27E-17
CRS 02		U1324C-6H-3WR	303.94	1940	0.47	7.28	−20.59	6.37E-18
CRS 03	X	U1324C-1H1-WR	51.21	1700	0.61	12.58	−23.93	4.95E-17
CRS 04	X	U1324C-1H-1WR	51.14	1700	0.61	9.36	−22.40	1.87E-17
CRS 05	X	U1324B-13H-7WR	117.40	1840	0.52	8.59	−21.31	1.57E-17
CRS 06		U1324B-70X-6WR	578.13	2080	0.38	8.72	−21.59	5.81E-19
CRS 07	X	U1324B-60X-2WR	476.86	2000	0.43	10.08	−22.24	1.28E-18
CRS 08		U1324C-7H-1WR	405.81	1830	0.53	8.60	−19.63	8.52E-16
CRS 13		U1324B-4H-7WR	32.14	1650	0.64	7.84	−21.28	5.01E-17
CRS 14		U1324B-4H-7WR	32.10	1650	0.64	7.29	−20.70	8.52E-17
CRS 15		U1324B-7H-7WR	60.62	1710	0.60	8.16	−20.95	8.87E-17
CRS 18		U1324B-26H-3WR	220.32	1900	0.49	-	-	-
CRS 19	X	U1324B-31H-3WR	261.02	1960	0.45	9.32	−21.18	1.14E-17
CRS 20		U1324B-21H-3WR	183.14	1920	0.48	9.81	−21.65	1.09E-17
CRS 797	X	U1324C-1H-1WR	51.27	1700	0.61	9.64	−22.66	1.52E-17
CRS 799	X	U1324C-1H-1WR	51.31	1700	0.61	10.38	−23.05	1.74E-17
CRS 800		U1324B-4H-7WR	31.86*	1630	0.65	7.53	−20.83	1.10E-16
CRS 801	X	U1324B-16H-5WR	142.13*	1940	0.47	7.49	−20.50	9.81E-18
CRS 802		U1324B-7H-7WR	60.31*	1720	0.59	8.36	−21.55	2.63E-17
CRS 803	X	U1324B-15H-5WR	134.20*	1900	0.49	7.76	−20.64	1.44E-17
CRS 807	X	U1324C-2H-4WR	105.48	1830	0.53	10.00	−22.03	1.88E-17
CRS 812		U1324B-23H-5WR	200.00	1910	0.48	11.75	−22.65	1.08E-17
CRS 813		U1324B-10H-7WR	89.22	1800	0.55	9.96	−22.06	2.49E-17

[a]Notes: CRS 08 sample = Ursa Siltstone, remaining samples = Ursa Mudstone.
[b]CRS Number: constant-rate-of-strain (CRS) consolidation test number.
[c]MTD: 'X' means the sample comes from a mass transport deposit (MTD).
[d]Depth: depth of the center of the whole core sample in mbsf; * depth of the core top only available.
[e]ρ_b: Logging-while-drilling (LWD) bulk density values from nearby where specimens were taken.
[f]n_i: in situ porosity calculated from logging-while-drilling bulk density log assuming grain density of 2740 kg/m^3 and water density of 1024 kg/m^3.
[g]γ: fitting parameter (slope of permeability-porosity relationship).
[h]log(k_0): fitting parameter (y-axis intercept of permeability-porosity relationship).
[i]k_i: in situ vertical permeability determined through extrapolation of individual log linear relationship between vertical permeability and porosity back to in situ porosity.

range (Figure 3). The overall trend between Ursa in situ permeabilities and in situ porosities follows the same log linear trend as observed for other natural mudstones such as marine mudstones from the Norwegian margin [*Yang and Aplin*, 1998], North Sea, Gulf of Mexico, and Caspian Sea [*Yang and Aplin*, 2007] (Figure 3, squares and upward pointing triangles). However, Ursa Mudstone samples document permeabilities at higher porosities because they were not buried as deeply as some of these other mudstones.

[18] The in situ permeability is higher for the Ursa Siltstone with a clay content of 32% than for the Ursa Mudstone with an average clay content of 60% (Figures 2 and 4). This dependence of permeability on clay content was also documented in the 1970s on samples from the Gulf of Mexico by *Bryant et al.* [1975], who divided their results into categories based on clay contents (Figure 3). However, we find no systematic relation between the mass fraction of the Ursa Mudstone that is smaller than 2 μm and the in situ permeability (Figures 4 and 5) [*Schneider*, 2011, Figure 3.9], which could result from small differences in composition or in sediment fabric. Similarly, neither specific surface area nor the presence or absence of MTDs shows a systematic variation with in situ permeability (Figure 6) [*Schneider*, 2011, Figures 3.10 and 3.11]. This is consistent with the observation that Ursa MTDs have similar porosity-resistivity relationships as the bounding, non-MTD sediments [*Dugan*, 2012]. *Dugan's* [2012] interpretation is that, despite changes in physical properties and petrophysical responses, MTD mobilization and emplacement has not significantly altered the fabric or general deformation behavior at the bed scale (0.1–1 m), and thus porosity-resistivity behavior, in these shallow sediments.

[19] During CRS testing, permeability is measured over a large porosity range. This allows the comparison of samples consolidated in the laboratory to samples that undergo compression during geological burial, if samples with similar composition yet from different burial depths are available. For example, a shallow sample (CRS 802, 60.31 mbsf; Figure 2, red dot) with the same clay fraction as the deepest sample (CRS 06, 578.13 mbsf; Figure 2, green dot) was compressed in the laboratory to almost the in situ porosity of the deepest sample (Figure 2, red line). By projecting the permeability-porosity trend of the shallow sample further to the in situ porosity of the deepest sample, the extrapolated

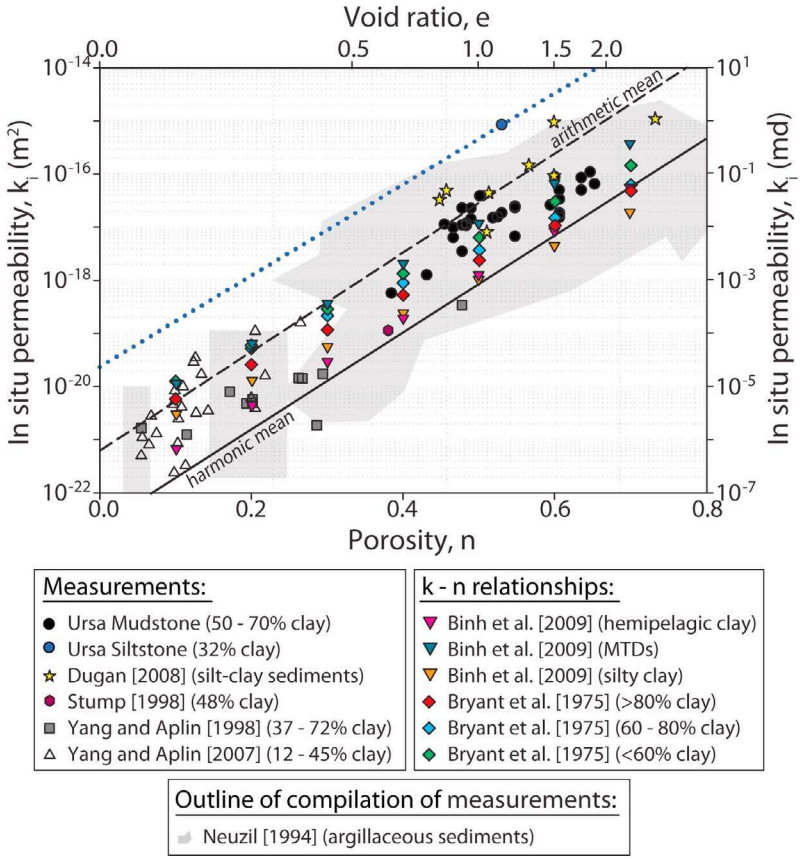

Figure 3. Comparison of in situ permeabilities (Table 2) with previously published vertical permeabilities. Permeabilities were measured using consolidation experiments [*Binh et al.*, 2009; *Bryant et al.*, 1975; *Dugan*, 2008], constant head technique [*Stump*, 1998], transient pulse decay technique [*Yang and Aplin*, 2007], and were calculated from a permeability model [*Yang and Aplin*, 1998]. Gray-shaded area shows compilation of permeability-porosity data of argillaceous sediments by *Neuzil* [1994]. All clay fractions except for *Stump* [1998] are defined as <2 μm. Dotted line- single Ursa Siltstone data set regression; dashed line- arithmetic mean of 30 Ursa Mudstone samples; solid line- harmonic mean of 30 Ursa Mudstone samples.

permeability of the laboratory-compressed sample is 0.8 times the in situ permeability of the deepest sample (Figure 2). This implies that, in this case of a "young" shallow system, we were able to reproduce how porosity and permeability of natural mudstone samples evolve near the seafloor over tens of thousands of years using consolidation experiments in the laboratory that last for a few days. However, over larger stresses and time ranges, where temperature and diagenesis act, that may not be the case. Our result is supported by *Long et al.* [2011] who showed that the in situ decline in porosity with increasing effective stress, of the same Ursa Basin samples as studied here, can be simulated in the laboratory by compressing a shallowly buried sample to a high effective stress. *Long et al.* [2011] interpreted that laboratory compression successfully reproduces the in situ compression behavior that occurs at much lower strain rates so that issues such as creep and cementation do not appear significant.

[20] In order to upscale our permeability measurements, we assume that permeability is transversely isotropic reflecting depositional layering and assume that our distribution of permeability measurements is statistically representative of the volumetric distribution of the facies present. Under these conditions, the vertical and horizontal permeability can be described by the harmonic and arithmetic mean, respectively [*Freeze and Cherry*, 1979; *Tegnander and Gimse*, 1998]. We calculate the harmonic and arithmetic mean for γ and $\log(k_0)$ of the 30 Ursa Mudstone samples and use the parameters to derive the upscaled vertical (equation (2)) and horizontal (equation (3)) permeability-porosity relationships as shown in Figure 2 and Table 3.

$$\log(k) = 9.10n - 22.63 \quad (2)$$

$$\log(k) = 9.29n - 21.21 \quad (3)$$

The harmonic mean preferentially weights the low-permeability layers and describes a lower bound on the measured permeabilities, whereas the arithmetic mean preferentially weights the high-permeability layers and describes an upper bound on the measured permeabilities (Figure 2). Most of the estimated in situ permeabilities lie, as expected, between the harmonic and arithmetic mean (Figures 2, 3, 4, and 5). We determine a permeability anisotropy, which is the ratio

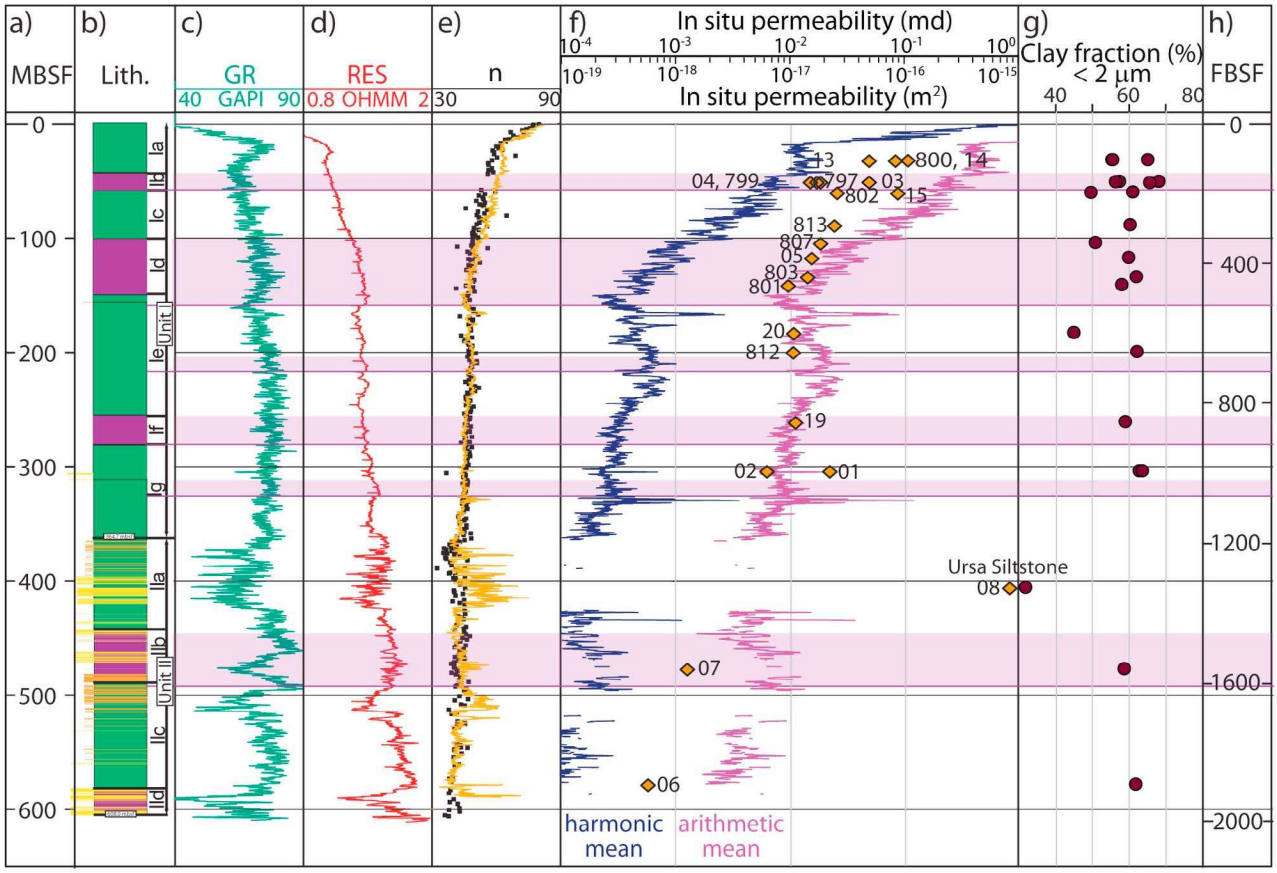

Figure 4. IODP Site U1324. (a) Depth in meters below seafloor (mbsf). (b) Lithology: Mass Transport Deposits (MTDs) (purple, shaded across all logs), siltstones (orange), sandstones (yellow), mudstones (green). (c) Gamma Ray (GR) from logging-while-drilling (LWD) data. (d) Resistivity (RES) log. (e) Porosity interpreted from shipboard moisture and density (MAD) measurements (solid symbols). Porosity interpreted from LWD bulk density log (orange line) assuming grain density of 2740 kg/m^3 and water density of 1024 kg/m^3. (f) In situ permeabilities (symbols) and harmonic (blue line) and arithmetic mean (purple line) of permeability-porosity relationships (calculated using log-derived porosity). CRS test numbers (orange diamonds). (g) Clay fraction (<2 μm) [*Sawyer et al.*, 2008]. (h) Depth in feet below seafloor (fbsf).

of horizontal to vertical permeability, by dividing the upscaled horizontal permeability (arithmetic mean of vertical permeability measurements) by the upscaled vertical permeability (harmonic mean of vertical permeability measurements). The resulting estimated large-scale permeability anisotropy decreases from 34.2 at a porosity of 0.6 to 30.0 at a porosity of 0.3 for the Ursa Mudstones. If we assume that any individual sample is isotropic, and the distribution of measurements is representative of the statistical variation in the rock at the larger scale, then our upscaled permeability anisotropy is an accurate estimate. However, if any individual sample has permeability anisotropy due to clay alignment [*Clennell et al.*, 1999], then our permeability anisotropy estimate is a conservative, or lower bound, estimate.

[21] In fact, the permeability anisotropy for individual samples is about 5 for a marine clay from off the coast of southern Chile (ODP Leg 141) [*Clennell et al.*, 1999], between 3 and 10 for clays and shales [*Freeze and Cherry*, 1979], and between 3 and 16 for sheared silty clays [*Dewhurst et al.*, 1996]. If we assume, based on these published values, that each of our samples has a permeability anisotropy of 5, then the upscaled permeability anisotropy is 39. This value is only slightly higher than the permeability anisotropy of 30–34 in the case of isotropic conditions.

[22] We explore whether our upscaled permeabilities are low enough to generate overpressure given the geologic forcing present in the Ursa Basin following the approach of *Neuzil* [1995]. Disequilibrium-type abnormal pressures exist when geologic processes perturb the pressure field at a rate exceeding the rate of pressure dissipation [*Neuzil*, 1995]. They are controlled by the size of the domain, the permeability of the domain, and the magnitude of the natural geologic processes, also called geologic forcing, such as compression or diagenesis [*Neuzil*, 1995]. *Neuzil* [1995] showed that abnormal pressures will be generated when the dimensionless geologic forcing (Γ_d) > 1, where Γ_d is the ratio of the product of geologic forcing (Γ) and characteristic length scale of the system (L) to the hydraulic conductivity (K).

[23] We calculate the geologic forcing for overpressure development in the Ursa Basin. We assume no diagenesis due to the shallow depths and low temperatures at Ursa, no fluid sources or sinks, and express the vertical loading term

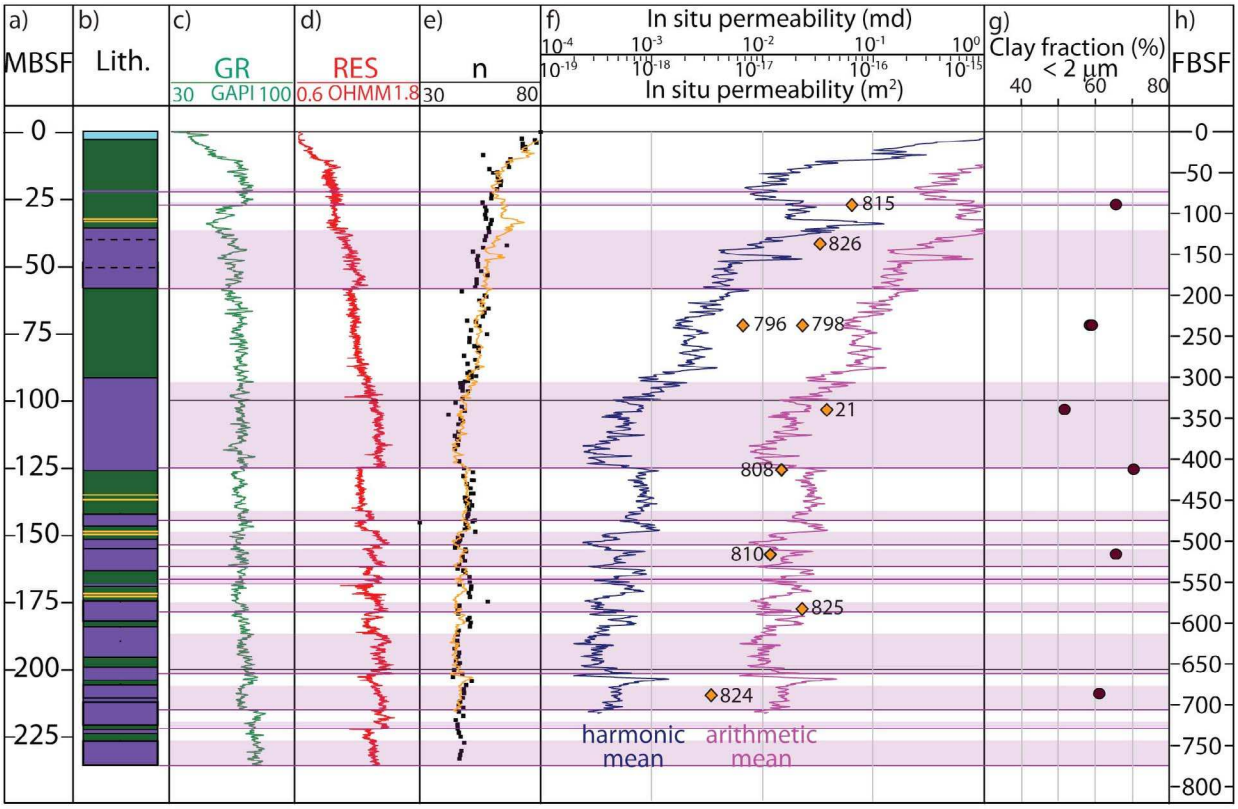

Figure 5. IODP Site U1322. (a) Depth in meters below seafloor (mbsf). (b) Lithology: Mass Transport Deposits (MTDs) (purple, shaded across all logs), siltstones (orange), sandstones (yellow), mudstones (green). (c) Gamma Ray (GR) from logging-while-drilling (LWD) data. (d) Resistivity (RES) log. (e) Porosity interpreted from shipboard moisture and density (MAD) measurements (solid symbols). Porosity interpreted from LWD bulk density log (orange line) assuming grain density of 2740 kg/m^3 and water density of 1024 kg/m^3. (f) In situ permeabilities (symbols) and harmonic (blue line) and arithmetic mean (purple line) of permeability-porosity relationships (calculated using log-derived porosity). CRS test numbers (orange diamonds). (g) Clay fraction (<2 μm) [*Sawyer et al.*, 2008]. (h) Depth in feet below seafloor (fbsf).

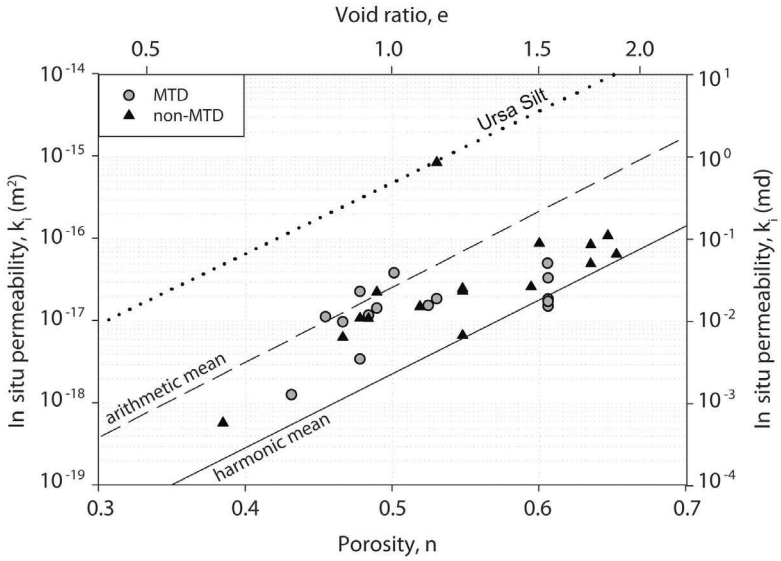

Figure 6. Comparison of in situ permeability-porosity relationships of samples from mass transport deposits (MTDs) (circles) and non-MTDs (triangles). Dotted line- single Ursa Siltstone data set regression; dashed line- arithmetic mean of 30 Ursa Mudstone samples; solid line- harmonic mean of 30 Ursa Mudstone samples.

Table 3. Parameters to Describe Permeability (k) vs. Porosity (n) Behavior[a]

Lithofacies	Equation (1)	
	$\log(k_0)$	γ
Ursa Mudstone (vertical permeability)	−22.63	9.10
Ursa Mudstone (horizontal permeability)	−21.21	9.29
Ursa Siltstone	−19.63	8.60

[a]Notes: vertical permeability determined by harmonic mean, horizontal permeability determined by arithmetic mean.

(compression) as δn/δt. For a sedimentation rate of 12 mm/yr (from Site U1324) [*Flemings et al.*, 2006, 2008, 2012], a geothermal gradient of 21°C/km [*Flemings et al.*, 2006], a porosity – vertical effective stress relationship determined by *Long et al.* [2011] (Figure 7a), and the harmonic mean (equation (2)) as the permeability-porosity relationship (Figure 7b and Table 3), we determine a geologic forcing for compression that decreases from 6×10^{-8} to 3×10^{-14} s^{-1} with increasing vertical effective stress. This range is noticeably higher than the value of 7×10^{-15} s^{-1} as used by *Neuzil* [1995] because of the high compressibility of shallow marine sediments. The dimensionless geologic forcing due to compression is greater than one below the depth of 5 mbsf (Figure 7e) indicating that abnormally high pore pressures can be generated in the Ursa Basin as documented by *Flemings et al.* [2008] and *Long et al.* [2011]. Further analysis of the terms show that Γ_d is less than 1 for thermal processes indicating that temperature is insignificant compared to compression (Figure 7e). Thus, permeability (Figure 7b) and compressibility (Figure 7c), therefore the coefficient of consolidation (Figure 7d), are important for overpressure development in the Ursa Basin, especially in the shallow section, but temperature is not.

[24] Based on our measured permeabilities, it is possible for us to estimate the upward fluid flow rates in the Ursa Basin. The observed abnormal pore pressures were directly measured near the seafloor and the pore pressure gradient is found to be 6.25 MPa/km at Site U1324 and 5 MPa/km at Site U1322 [*Flemings et al.*, 2008]. Using the upscaled vertical permeability relationship (equation (2)) and assuming a porosity of 0.55 at a depth of 100 mbsf at Site U1324 and a porosity of 0.47 at 100 mbsf at Site U1322, we find that vertical fluid flow rates in the mudstones are 0.5 mm/yr at Site U1324 and 0.07 mm/yr at Site U1322 based on Darcy's Law. Average seawater density (1024 kg/m^3) and constant dynamic viscosity (0.001 Pa s) are assumed. These upward fluid flow rates are smaller but within the same ballpark as upward flow rates of approximately 4 mm/yr determined in clay- and silt-size sediments from the approximately 400 km away Keathley Canyon, northern Gulf of Mexico [*Dugan*,

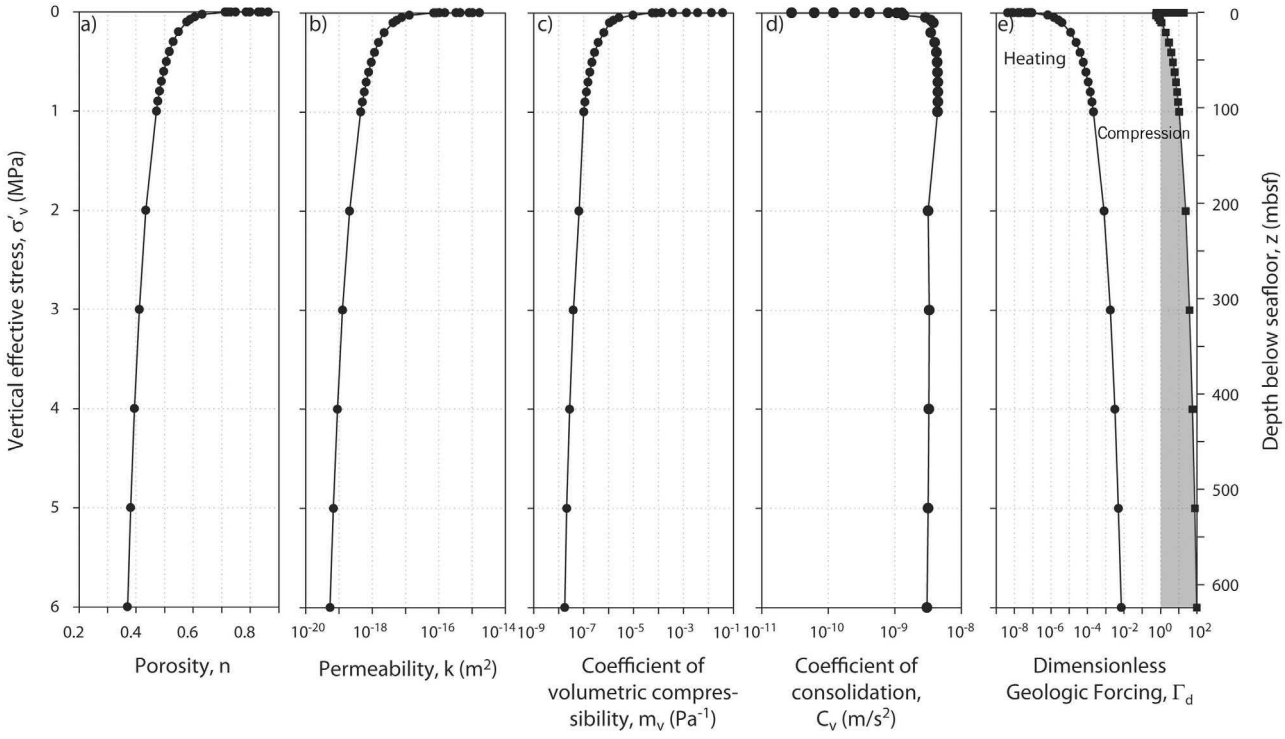

Figure 7. Series of estimated properties for Ursa Mudstones versus vertical effective stress (axis label at left) and depth below seafloor (axis label at right). (a) porosity estimated from vertical effective stress using relationship established by *Butterfield* [1979] and applied to Ursa Mudstones by *Long et al.* [2011], (b) permeability estimated from porosity using harmonic mean (equation (2)), (c) coefficient of volumetric compressibility, (d) coefficient of consolidation, and (e) absolute value of dimensionless geologic forcing as defined in *Neuzil* [1995] due to heating (circles) and compression (squares). Shaded area refers to depth/stress range where absolute value of dimensionless geologic forcing due to compression is >1, which suggests that abnormal pressures can be generated [*Neuzil*, 1995].

2008] and with existing regional-scale flow models in the northern Gulf of Mexico [*Stigall and Dugan*, 2010]. The upward fluid flow rates in Keathley Canyon were estimates made from consolidation experiments, logging-while-drilling data, and drilling observations. In contrast, at Ursa we can confidently derive upward fluid flow rates because permeability as well as pore fluid pressures are well constrained. This has seldom, if ever, been documented and is one of the first constraints of active fluid flow in shallow, low permeability systems.

5. Conclusions

[25] Vertical permeabilities of Ursa Mudstones and Ursa Siltstone from Sites U1324 and U1322 in the Ursa Basin, Gulf of Mexico, vary over orders of magnitude at a given porosity. We quantify the permeability-porosity relationship for 31 Ursa Mudstone and Ursa Siltstone samples, and use these relationships to derive in situ permeabilities that decrease with porosity similar to the experimentally derived permeability-porosity trend. Thus, we are able to reproduce how porosity and permeability of natural mudstone samples evolve over tens of thousands of years using consolidation experiments in the laboratory that last for a few days. We use harmonic and arithmetic means to upscale discrete permeability measurements taken at various depths to larger-scale vertical and horizontal permeabilities as well as to determine a large-scale permeability anisotropy. Based on these upscaled permeabilities we show that overpressure should have been generated at Ursa, and direct measurements confirm this interpretation. Based on the magnitude of these known overpressure gradients and our permeability functions, we calculate upward fluid flow rates of 0.07 to 0.5 mm/yr within the mudstones of the Ursa Basin.

[26] **Acknowledgments.** We thank the crew, technicians, and scientific staff of the *JOIDES Resolution* for their extraordinary efforts during IODP Expedition 308. This project was funded by the UT GeoFluids consortium at The University of Texas at Austin, www.beg.utexas.edu/geofluids/index (supported by 11 energy companies). This research used samples and data provided by the Integrated Ocean Drilling Program (IODP). IODP is sponsored by the U.S. National Science Foundation (NSF) and participating countries, and administered by the Consortium for Ocean Leadership Inc. The samples tested at The Pennsylvania State University were run in Demian Saffer's Sediment & Rock Mechanics laboratory. Publication is authorized by the Director, Bureau of Economic Geology, The University of Texas. This paper is The University of Texas Institute for Geophysics contribution 2497.

References

Adatia, R. H., and A. J. Maltman (2004), Data report: Initial permeability determinations on sediments from the Nankai Trough accretionary prism, ODP Sites 1173 and 1174, *Proc. Ocean Drill. Program Sci. Results*, *190/196*, 12 pp., doi:10.2973/odp.proc.sr.190196.214.2004.

Amann-Hildenbrand, A., A. Ghanizadeh, and B. M. Krooss (2012), Transport properties of unconventional gas systems, *Mar. Pet. Geol.*, *31*, 90–99, doi:10.1016/j.marpetgeo.2011.11.009.

ASTM International (2006), Standard test method for one-dimensional consolidation properties of saturated cohesive soils using controlled-strain loading (Standard D4186-06), in *Annual Book of ASTM Standards*, vol. 04.08, 15 pp., Am. Soc. for Testing and Mater., West Conshohocken, Penn., doi:10.1520/D4186-06.

Berndt, C., S. Bünz, and J. Mienert (2003), Polygonal fault systems on the mid-Norwegian margin: A long-term source of fluid flow, in *Subsurface Sediment Mobilization*, edited by P. Van Rensbergen et al., *Geol. Soc. Spec. Publ.*, *216*, 283–290, doi:10.1144/GSL.SP.2003.216.01.18.

Bethke, C. M., and T. Corbet (1988), Linear and non-linear solutions for one-dimensional compaction flow in sedimentary basins, *Water Resour. Res.*, *24*, 461–467, doi:10.1029/WR024i003p00461.

Billiotte, J., D. Yang, and K. Su (2008), Experimental study on gas permeability of mudstones, *Phys. Chem. Earth*, *33*, S231–S236, doi:10.1016/j.pce.2008.10.040.

Binh, N. T. T., T. Tokunaga, T. Nakamura, K. Kozumi, M. Nakajima, M. Kubota, H. Kameya, and M. Taniue (2009), Physical properties of the shallow sediments in late Pleistocene formations, Ursa Basin, Gulf of Mexico, and their implications for generation and preservation of shallow overpressures, *Mar. Pet. Geol.*, *26*(4), 474–486, doi:10.1016/j.marpetgeo.2009.01.018.

Blum, P. (1997), Physical properties handbook: A guide to the shipboard measurement of physical properties of deep-sea cores, *ODP Tech. Note 26*, Ocean Drill. Program, College Station, Tex., doi:10.2973/odp.tn.26.1997.

Bourlange, S., L. Jouniaux, and P. Henry (2004), Data report: Permeability, compressibility, and friction coefficient measurements under confining pressure and strain, Leg 190, Nankai Trough, *Proc. Ocean Drilling Program Sci. Results*, *190*, 16 pp., doi:10.2973/odp.proc.sr.190196.215.204.

Bryant, W. R. (2002), Permeability of clays, silty-clays and clayey-silts, *Gulf Coast Assoc. Geol. Soc. Trans.*, *52*, 1069–1077.

Bryant, W. R., W. Hottman, and P. Trabant (1975), Permeability of unconsolidated and consolidated marine sediments, Gulf of Mexico, *Mar. Geotechnol.*, *1*, 1–14, doi:10.1080/10641197509388149.

Bryant, W. R., A. Wetzel, E. Taylor, and W. Sweet (1986), Consolidation characteristics and permeability of Mississippi Fan sediments, *Initial Rep. Deep Sea Drill. Program*, *96*, 797–809, doi:10.2973/dsdp.proc.96.151.1986.

Butterfield, R. (1979), A natural compression law for soils (an advance on e-logp'), *Geotechnique*, *29*, 469–480, doi:10.1680/geot.1979.29.4.469.

Carman, P. C. (1937), Flow through a granular bed, *Trans. Inst. Chem. Eng. London*, *15*, 150–156.

Clennell, M. B., D. N. Dewhurst, K. M. Brown, and G. K. Westbrook (1999), Permeability anisotropy of consolidated and unconsolidated clays, in *Muds and Mudstones: Physical and Fluid Flow Properties*, edited by A. C. Aplin, A. J. Fleet, and J. H. S. Macquaker, *Geol. Soc. Spec. Publ.*, *158*, 79–96.

Cui, X., A. M. M. Bustin, and R. M. Bustin (2009), Measurements of gas permeability and diffusivity of tight reservoir rocks: Different approaches and their applications, *Geofluids*, *9*, 208–223, doi:10.1111/j.1468-8123.2009.00244.x.

Dewhurst, D. N., K. M. Brown, M. B. Clennell, and G. K. Westbrook (1996), A comparison of the fabric and permeability anisotropy of consolidated and sheared silty clay, *Eng. Geol. Amsterdam*, *42*(4), 253–267, doi:10.1016/0013-7952(95)00089-5.

Dugan, B. (2008), Fluid flow in the Keathley Canyon 151 Mini-Basin, northern Gulf of Mexico, *Mar. Pet. Geol.*, *25*(9), 919–923, doi:10.1016/j.marpetgeo.2007.12.005.

Dugan, B. (2012), Petrophysical and consolidation behavior of mass transport deposits from the northern Gulf of Mexico, IODP Expedition 308, *Mar. Geol.*, *315–318*, 98–107, doi:10.1016/j.margeo.2012.05.001.

Dugan, B., and P. B. Flemings (2000), Overpressure and fluid flow in the New Jersey continental slope: Implications for slope failure and cold seeps, *Science*, *289*(5477), 288–291, doi:10.1126/science.289.5477.288.

Dugan, B., and P. B. Flemings (2002), Fluid flow and stability of the US continental slope offshore New Jersey from the Pleistocene to the present, *Geofluids*, *2*, 137–146, doi:10.1046/j.1468-8123.2002.00032.x.

Dugan, B., and J. Germaine (2008), Near-seafloor overpressure in the deepwater Mississippi Canyon, northern Gulf of Mexico, *Geophys. Res. Lett.*, *35*, L02304, doi:10.1029/2007GL032275.

Fisher, A. T., and G. Zwart (1997), Packer experiments along the decollement of the Barbados accretionary complex: Measurements of in situ permeability, *Proc. Ocean Drill. Program Sci. Results*, *156*, 199–218, doi:10.2973/odp.proc.sr.156.027.1997.

Fisher, A. T., K. Fischer, D. Lavoie, M. Langseth, and J. Xu (1994), Geotechnical and hydrogeological properties of sediments from Middle Valley, northern Juan de Fuca Ridge, *Proc. Ocean Drill. Program Sci. Results*, *139*, 627–647, doi:10.2973/odp.proc.sr.139.246.1994.

Flemings, P. B., J. H. Behrmann, and C. M. John, and the Expedition 308 Scientists (2006), *Gulf of Mexico Hydrogeology*, *Proc. Integrated Ocean Drill. Program*, vol. 308, Integrated Ocean Drill. Program, College Station, Tex., doi:10.2204/iodp.proc.308.2006.

Flemings, P. B., H. Long, B. Dugan, J. T. Germaine, C. John, J. H. Behrmann, D. E. Sawyer, and E. Scientists (2008), Erratum to "Pore pressure penetrometers document high overpressure near the seafloor where multiple submarine landslides have occurred on the continental slope, offshore Louisiana, Gulf of Mexico," *Earth Planet. Sci. Lett.*, *274*, 269–283, doi:10.1016/j.epsl.2008.06.027.

Flemings, P. B., C. John, and J. H. Behrmann (2012), Expedition 308 synthesis: Overpressure, consolidation, and slope stability on the continental slope of the Gulf of Mexico, in *Gulf of Mexico Hydrogeology*, *Proc. Integrated Ocean Drill. Program*, *308*, doi:10.2204/iodp.proc.308.215.2012.

Freeze, R. A., and J. A. Cherry (1979), *Groundwater*, 604 pp., Prentice Hall, Englewood Cliffs, N. J.

Gamage, K., and E. Screaton (2003), Data report: Permeabilities of Nankai accretionary prism sediments, *Proc. Ocean Drill. Program Sci. Results*, *190/196*, 22 pp., doi:10.2973/odp.proc.sr.190196.213.2003.

Gamage, K., B. Bekins, and E. Screaton (2005), Data report: Permeabilities of eastern equatorial Pacific and Peru margin sediments, *Proc. Ocean Drill. Program Sci. Results*, *201*, 18 pp., doi:10.2973/odp.proc.sr.201.103.2005.

Gamage, K., E. Screaton, B. Bekins, and I. Aiello (2011), Permeability-porosity relationships of subduction zone sediments, *Mar. Geol.*, *279*, 19–36, doi:10.1016/j.margeo.2010.10.010.

Gibson, R. E. (1958), The progress of consolidation in a clay layer increasing in thickness with time, *Geotechnique*, *8*, 171–182, doi:10.1680/geot.1958.8.4.171.

Hermanrud, C. (1993), Basin modeling techniques—An overview, in *Basin Modelling: Advances and Applications*, *Norw. Pet. Soc. Spec. Publ.*, vol. 3, edited by A. G. Doré, pp. 1–34, Elsevier, New York.

Kozeny, J. (1927), Über kapillare Leitung des Wassers im Boden - Aufstieg, Versickerung und Anwendung auf die Bewässerung, *Sitzungsber. Akad. Wiss. Wien*, *136*, 271–306.

Long, H., P. B. Flemings, J. T. Germaine, D. M. Saffer, and B. Dugan (2008), Data report: Consolidation characteristics of sediments from IODP Expedition 308, Ursa Basin, Gulf of Mexico, *Proc. Ocean Drill. Program Sci. Results*, *308*, 47 pp., doi:10.2204/iodp.proc.308.204.2008.

Long, H., P. B. Flemings, J. T. Germaine, and D. M. Saffer (2011), Consolidation and overpressure near the seafloor in the Ursa Basin, deepwater Gulf of Mexico, *Earth Planet. Sci. Lett.*, *305*, 11–20, doi:10.1016/j.epsl.2011.02.007.

Luffel, D. L., C. W. Hopkins, and P. D. Schettler Jr. (1993), Matrix permeability measurements of gas productive shales, in *68th Annual Technical Conference and Exhibition of the Society of Petroleum Engineers*, pp. 261–270, Soc. of Pet. Eng., Richardson, Tex.

McKiernan, A. W., and D. M. Saffer (2006), Data report: Permeability and consolidation properties of subducting sediments off Costa Rica, ODP Leg 205, *Proc. Ocean Drill. Program Sci. Results*, *205*, 24 pp., doi:10.2973/odp.proc.sr.205.203.2006.

Neuman, S. P. (1994), Generalized scaling of permeabilities: Validation and effect of support scale, *Geophys. Res. Lett.*, *21*(5), 349–352, doi:10.1029/94GL00308.

Neuzil, C. E. (1994), How permeable are clays and shales?, *Water Resour. Res.*, *30*(2), 145–150, doi:10.1029/93WR02930.

Neuzil, C. E. (1995), Abnormal pressures as hydrodynamic phenomena, *Am. J. Sci.*, *295*(6), 742–786, doi:10.2475/ajs.295.6.742.

Paull, C. K., W. Ussler III, W. S. Holbrook, T. M. Hill, R. Keaten, J. Mienert, H. Haflidason, J. E. Johnson, W. J. Winters, and T. D. Lorenson (2008), Origin of pockmarks and chimney structures on the flanks of the Storegga Slide, offshore Norway, *Geo Mar. Lett.*, *28*, 43–51, doi:10.1007/s00367-007-0088-9.

Prior, D. B., and J. M. Coleman (1982), Active slides and flows in underconsolidated marine sediments on the slope of the Mississippi delta, in *Marine Slides and Other Mass Movements*, edited by S. Saxov and J. K. Nieuwenhuis, pp. 21–49, Plenum, New York, doi:10.1007/978-1-4613-3362-3_3.

Prior, D. B., and J. N. Suhayda (1979), Application of infinite slope analysis to subaqueous sediment instability, Mississippi delta, *Eng. Geol. Amsterdam*, *14*(1), 1–10, doi:10.1016/0013-7952(79)90059-0.

Rubin, Y., and J. J. Gomez-Hernandez (1990), A stochastic approach to the problem of upscaling of conductivity in disordered media: Theory and unconditional numerical simulations, *Water Resour. Res.*, *26*(4), 691–701, doi:10.1029/WR026i004p00691.

Ruppel, C., G. R. Dickens, D. G. Castellini, W. Gilhooly, and D. Lizarralde (2005), Heat and salt inhibition of gas hydrate formation in the northern Gulf of Mexico, *Geophys. Res. Lett.*, *32*, L04605, doi:10.1029/2004GL021909.

Saffer, D. M., and B. A. Bekins (2002), Hydrologic controls on the morphology and mechanics of accretionary wedges, *Geology*, *30*(3), 271–274, doi:10.1130/0091-7613(2002)030<0271:HCOTMA>2.0.CO;2.

Saffer, D. M., and B. A. Bekins (2006), An evaluation of factors influencing pore pressure in accretionary complexes: Implications for taper angle and wedge mechanics, *J. Geophys. Res.*, *111*, B04101, doi:10.1029/2005JB003990.

Saffer, D. M., and A. W. McKiernan (2005), Permeability of underthrust sediments at the Costa Rican subduction zone: Scale dependence and implications for dewatering, *Geophys. Res. Lett.*, *32*, L02302, doi:10.1029/2004GL021388.

Saffer, D. M., E. A. Silver, A. T. Fisher, H. Tobin, and K. Moran (2000), Inferred pore pressures at the Costa Rica subduction zone: Implications for dewatering processes, *Earth Planet. Sci. Lett.*, *177*(3–4), 193–207, doi:10.1016/S0012-821X(00)00048-0.

Saffer, D., J. Guo, M. B. Underwood, W. Likos, R. M. Skarbek, I. Song, and M. Gildow (2011), Data report: Consolidation, permeability, and fabric of sediments from the Nankai continental slope, IODP Sites C0001, C0008, and C0004, *Proc. Ocean Drill. Program Sci. Results*, *314/315/316*, 58 pp., doi:10.2204/iodp.proc.314315316.218.2011.

Sawyer, D. E., P. B. Flemings, R. C. Shipp, and C. D. Winker (2007), Seismic geomorphology, lithology, and evolution of the late Pleistocene Mars-Ursa turbidite region, Mississippi Canyon area, northern Gulf of Mexico, *AAPG Bull.*, *91*(2), 215–234, doi:10.1306/08290605190.

Sawyer, D. E., R. Jacoby, P. B. Flemings, and J. T. Germaine (2008), Data report: Particle size analysis of sediments in the Ursa Basin, IODP Expedition 308 Sites U1324 and U1322, northern Gulf of Mexico, *Proc. Ocean Drill. Program Sci. Results*, *308*, 20 pp., doi:10.2204/iodp.proc.308.205.2008.

Sawyer, D. E., P. B. Flemings, B. Dugan, and J. T. Germaine (2009), Retrogressive failures recorded in mass transport deposits in the Ursa Basin, northern Gulf of Mexico, *J. Geophys. Res.*, *114*, B10102, doi:10.1029/2008JB006159.

Scheidegger, A. (1974), *The Physics of Flow Through Porous Media*, Univ. of Toronto Press, Toronto, Ont., Canada, doi:10.1097/00010694-195812000-00015.

Schneider, J. (2011), Compression and permeability behavior of natural mudstones, PhD thesis, 321 pp., Univ. of Tex. at Austin, Austin.

Screaton, E. J., D. R. Wuthrich, and S. J. Dreiss (1990), Permeabilities, fluid pressures, and flow rates in the Barbados Ridge Complex, *J. Geophys. Res.*, *95*(B6), 8997–9007, doi:10.1029/JB095iB06p08997.

Screaton, E., T. Hays, K. Gamage, and J. Martin (2006), Data report: Permeabilities of Costa Rica subduction zone sediments, *Proc. Ocean Drill. Program Sci. Results*, *205*, 13 pp., doi:10.2973/odp.proc.sr.205.204.2006.

Sheahan, T. C., and P. J. Watters (1997), Experimental verification of CRS consolidation theory, *J. Geotech. Geoenviron. Eng.*, *123*(5), 430–437, doi:10.1061/(ASCE)1090-0241(1997)123:5(430).

Skarbek, R. M., and D. M. Saffer (2009), Pore pressure development beneath the décollement at the Nankai subduction zone: Implications for plate boundary fault strength and sediment dewatering, *J. Geophys. Res.*, *114*, B07401, doi:10.1029/2008JB006205.

Smith, R. E., and H. E. Wahls (1969), Consolidation under constant rates of strain, *J. Soil Mech. Found. Div. Am. Soc. Civ. Eng.*, *96*(2), 519–539.

Spinelli, G. A., E. R. Giambalvo, and A. T. Fisher (2004a), Sediment permeability, distribution, and influence on fluxes in oceanic basement, in *Hydrogeology of the Oceanic Lithosphere*, edited by E. E. Davis and H. Elderfield, pp. 151–188, Cambridge Univ. Press, Cambridge, U. K.

Spinelli, G. A., L. Zühlsdorff, A. T. Fisher, C. G. Wheat, M. Mottl, V. Spieß, and E. R. Giambalvo (2004b), Hydrothermal seepage patterns above a buried basement ridge, eastern flank of the Juan de Fuca Ridge, *J. Geophys. Res.*, *109*, B01102, doi:10.1029/2003JB002476.

Stigall, J., and B. Dugan (2010), Overpressure and earthquake initiated slope failure in the Ursa region, northern Gulf of Mexico, *J. Geophys. Res.*, *115*, B04101, doi:10.1029/2009JB006848.

Stump, B. B. (1998), Illuminating basinal fluid flow in Eugene Island 330 (Gulf of Mexico) through in situ observations, deformation experiments, and hydrodynamic modeling, Master's thesis, 121 pp., Penn. State Univ., Univ. Park.

Tan, B., J. T. Germaine, and P. B. Flemings (2006), Data report: Consolidation and strength characteristics of sediments from ODP Site 1244, Hydrate Ridge, Cascadia continental margin, *Proc. Ocean Drill. Program Sci. Results*, *204*, 148 pp., doi:10.2973/odp.proc.sr.204.102.2006.

Taylor, E., and A. Fisher (1993), Sediment permeability at the Nankai accretionary prism, Site 808, *Proc. Ocean Drill. Program Sci. Results*, *131*, 235–245, doi:10.2973/odp.proc.sr.131.131.1993.

Taylor, E., and J. Leonard (1990), Sediment consolidation and permeability at the Barbados Forearc, *Proc. Ocean Drill. Program Sci. Results*, *110*, 289–308, doi:10.2973/odp.proc.sr.110.152.1990.

Tegnander, C., and T. Gimse (1998), Flow simulations to evaluate upscaling of permeability, *J. Math. Geol.*, *30*(6), 717–731, doi:10.1023/A:1022347403212.

Vidstrand, P. (2001), Comparison of upscaling methods to estimate hydraulic conductivity, *Ground Water*, *39*(3), 401–407, doi:10.1111/j.1745-6584.2001.tb02324.x.

Winker, C. D., and J. R. Booth (2000), Sedimentary dynamics of the salt-dominated continental slope, Gulf of Mexico: Integration of observations from the seafloor, near-surface, and deep subsurface, in *GCSSEPM Foundation Bob F. Perkins 20th Annual Research Conference*, edited by P. Weimar et al., pp. 1059–1086, Gulf Coast Sect. Soc. of Econ. Paleontol. and Mineral. Found., Houston, Tex.

Winker, C. D., and R. C. Shipp (2002), Sequence stratigraphic framework for prediction of shallow water flow in the Greater Mars-Ursa Area, Mississippi Canyon Area, Gulf of Mexico Continental Slope, in *22nd Annual GCSSEPM Foundation Bob F. Perkins Research Conference*, edited by J. M. Armentrout and N. C. Rosen, p. 42, Gulf Coast Sect. Soc. of Econ. Paleontol. and Mineral. Found., Houston, Tex.

Yang, Y. L., and A. C. Aplin (1998), Influence of lithology and compaction on the pore size distribution and modelled permeability of some

mudstones from the Norwegian margin, *Mar. Pet. Geol.*, *15*, 163–175, doi:10.1016/S0264-8172(98)00008-7.

Yang, Y. L., and A. C. Aplin (2007), Permeability and petrophysical properties of 30 natural mudstones, *J. Geophys. Res.*, *112*, B03206, doi:10.1029/2005JB004243.

Zwart, G., W. Brückmann, K. Moran, A. K. MacKillop, A. J. Maltman, A. Bolton, P. Vrolijk, T. Miller, M. J. Gooch, and A. Fisher (1997), Evaluation of hydrogeologic properties of the Barbados accretionary prism: A synthesis of Leg 156 results, *Proc. Ocean Drill. Program Sci. Results*, *156*, 303–310, doi:10.2973/odp.proc.sr.156.036.1997.